

# Using Scaled Embedded Distances to Generate Metrics for $\mathbb{R}^2$

By Mario Kapl<sup>1</sup>, Franz Aurenhammer<sup>2</sup>, and Bert Jüttler<sup>1</sup>

<sup>1</sup>Institute of Applied Geometry, Johannes Kepler University, Linz, Austria

<sup>2</sup>Institute for Theoretical Computer Science, University of Technology, Graz, Austria

## Abstract

A metric on a set  $A$  is a symmetric function which defines a nonnegative distance between any two points of  $A$ , such that the triangle inequality is fulfilled. Given a set of points, called sites, the metric can be used to generate Voronoi diagrams which capture the nearest point information.

We present a new class of metrics on  $\mathbb{R}^2$ , which we call the scaled embedding-generated (SEG) metric. These metrics are defined with the help of a smooth one-to-one embedding of  $\mathbb{R}^2$  into  $\mathbb{R}^m$  and an additional scalar-valued function which is used to re-scale the distances.

We describe a possible construction of an SEG metric which is based on the Gauß-Newton algorithm. More precisely, we show how to generate a spline embedding, which approximates a given distance graph on a finite set of points in  $\mathbb{R}^2$ , in the sense of least squares. Distances are required to satisfy the generalized polygon inequality.

The framework is used to define a new type of Voronoi diagram in  $\mathbb{R}^2$ , which is possibly anisotropic as it allows for different distance functions for the sites. We explain a simple method to compute such Voronoi diagrams. Several examples of diagrams resulting from different SEG metrics are presented.

## 1. Introduction

The Voronoi diagram of a finite set of points (or more general sites) is a powerful and popular concept in geometry which possesses a wide range of applications, e.g. to motion planning, geometrical clustering and meshing; cf. Aurenhammer & Klein (2000) and Okabe et al. (2000). The classical Voronoi diagram uses the Euclidean metric to define distances. One possible approach to generalize this setting is to use different distance functions to generate the Voronoi cells. This concept has led to a large number of different types of Voronoi diagrams described in the literature.

As a first example relevant to the present paper, we outline the idea of an anisotropic Voronoi diagram in Labelle & Shewchuk (2003). For each point  $p$  (in  $\mathbb{R}^2$ ), a different metric is defined, which specifies the distance to all other points in  $\mathbb{R}^2$ , as seen from  $p$ . The distance between two points is then given as the minimum of the two distances resulting from their associated metrics. This distance is not a metric, in general, because the triangle inequality need not be satisfied. However, this is no serious hinderance for computing the anisotropic Voronoi diagram. The corresponding Voronoi cells can be generated only with the help of the associated metrics for the given *sites*.

A similar concept is explained in Du & Wang (2005), where an anisotropic metric field is used to define for each point  $p \in \mathbb{R}^2$  a possibly different anisotropic distance function. In contrast to Labelle & Shewchuk (2003), the Voronoi cells are computed by using the

complete metric field. Once again, the distance between two points does not define a metric since this distance is not symmetric, in general.

Both types of anisotropic Voronoi diagrams can be seen as generalizations of the weighted Voronoi diagram in Aurenhammer & Edelsbrunner (1984), where for each site a multiplicatively weighted Euclidean distance is used. Further works following these or similar anisotropic approaches are Boissonnat, Wormser & Yvinec (2007) and (2008), Letscher (2007), Canas & Gortler (2011a) and (2011b), and Canas (2012).

A different idea for the construction of an anisotropic Voronoi diagram is presented in Kunze, Wolter & Rausch (1997). A Voronoi diagram on a parametric surface is generated, where the distances between the points on the surface are given by the corresponding geodesic distances. By considering the resulting Voronoi diagram in the parameter domain of the surface we obtain a Voronoi diagram, which is possibly anisotropic. However, the computation of this Voronoi diagram is rather expensive, since it requires the frequent evaluation of geodesic distances on a parametric surface.

In the present paper we introduce a new metric framework on  $\mathbb{R}^2$ , called scaled embedding-generated metric (SEG metric), which is used to define an anisotropic type of a Voronoi diagram. The new metric is defined with the help of an embedding of  $\mathbb{R}^2$  into a higher-dimensional space. The distance of two points in  $\mathbb{R}^2$  is given by the (weighted) Euclidean distance of the two corresponding points on the resulting surface. As one possible way to construct a suitable embedding, a method is explained where the embedding is generated from a distance graph via a fitting procedure.

The construction of the SEG metric Voronoi diagram has several advantages. We have only one distance function for all points which indeed defines a metric on  $\mathbb{R}^2$ . Moreover, the computation of the distances is fast and simple. Also, some properties of the SEG metric Voronoi diagrams can be derived from the properties of the Euclidean Voronoi diagram in  $\mathbb{R}^2$  and  $\mathbb{R}^3$ .

This paper is organized as follows. Section 2 recalls some basic concepts, including the Voronoi diagram, the medial axis, and the local feature size for the Euclidean metric. Section 3 describes the SEG metric setting mentioned above, which is based on a smooth and injective embedding of  $\mathbb{R}^2$  into  $\mathbb{R}^m$  for  $m \geq 2$  and a scalar-valued function. In the case of  $m = 2$  and  $m = 3$ , the embedding is just a parametric surface without self-intersections in  $\mathbb{R}^2$  and  $\mathbb{R}^3$ , respectively.

In Section 4 we describe a method for constructing a SEG metric from a given distance graph. The creation of the associated spline embedding is based on the Gauß-Newton algorithm, a well known iterative method to solve non-linear least-squares problems. If the distance graph satisfies the generalized polygon inequality, the embedding surface is capable of approximating distances very accurately. Several examples of SEG metrics resulting from different distance graphs are presented.

An application of the introduced framework is described in Section 5. We use the SEG metric to define a generalized Voronoi diagram, and give conditions under which the resulting Voronoi cells stay connected. Several examples of such Voronoi diagrams for different SEG metrics are given, computed with the help of our algorithm.

## 2. Preliminaries

We give a short overview of the concepts of Voronoi diagrams, medial axes, and local feature size. We will later, in Section 5, generalize Voronoi diagrams with the help of the metrics specified in Section 3. The concept of local feature size will be needed to describe some properties of the SEG metrics and of the resulting SEG metric Voronoi diagrams.

### 2.1. Voronoi diagram

Let  $\mathbf{P} = \{\mathbf{p}_1, \mathbf{p}_2, \dots\}$  be a finite set of points (called sites) in Euclidean  $m$ -space  $\mathbb{R}^m$ , for  $m \geq 2$ . For a given metric  $D$  on  $\mathbb{R}^m$ , we define the Voronoi cell,  $V_D^i(\mathbf{P})$ , of a site  $\mathbf{p}_i \in \mathbf{P}$  as the open set

$$V_D^i(\mathbf{P}) = \{\mathbf{p} \in \mathbb{R}^m \mid D(\mathbf{p}, \mathbf{p}_i) < D(\mathbf{p}, \mathbf{p}_j) \text{ for all } j \neq i\}.$$

The Voronoi diagram,  $V_D(\mathbf{P})$ , is now given by the complement of all Voronoi regions in  $\mathbb{R}^m$ ,

$$V_D(\mathbf{P}) = \mathbb{R}^m \setminus \left( \bigcup_i V_D^i(\mathbf{P}) \right).$$

We denote the Voronoi diagram with respect to the Euclidean metric by  $V(\mathbf{P})$ . A Voronoi diagram is called orphan-free if each of its Voronoi cells is connected. In the case of the Euclidean metric, the diagram is always orphan-free, because its regions are intersections of open halfspaces of  $\mathbb{R}^m$ , and thus are convex polyhedra.

### 2.2. Medial axis

Let  $\mathbf{x} : \mathbb{R}^2 \rightarrow \mathbb{R}^m$ , for  $m \geq 2$ , be a continuous one-to-one embedding with

$$\mathbf{x}(u, v) = (x_1(u, v), \dots, x_m(u, v)).$$

Consider the set  $\mathbf{X} = \mathbf{x}(\mathbb{R}^2)$  of all image points of the embedding  $\mathbf{x}(u, v)$ . We define the medial axis of  $\mathbf{X}$  as the (closure of the) set of all points in  $\mathbb{R}^m$  that have at least two closest points in  $\mathbf{X}$ .

An equivalent definition could be given as follows. A ball  $B_r(\mathbf{c}) \subset \mathbb{R}^m$  with radius  $r > 0$  and center  $\mathbf{c} \in \mathbb{R}^m$  is given by

$$B_r(\mathbf{c}) = \{\mathbf{p} \in \mathbb{R}^m \mid \|\mathbf{p} - \mathbf{c}\| \leq r\}.$$

Such a ball is called empty with respect to  $\mathbf{X}$  if the interior of  $B_r(\mathbf{c})$  contains no points of  $\mathbf{X}$ . We say that  $B_r(\mathbf{c})$  is a medial ball if it is maximal with respect to  $\mathbf{X}$ , i.e., if no other empty ball  $B$  with  $B \neq B_r(\mathbf{c})$  and containing  $B_r(\mathbf{c})$  exists. The set of centers of all medial balls for  $\mathbf{X}$  form the medial axis of  $\mathbf{X}$ .

### 2.3. Local feature size

We explain the concept of local feature size, which was introduced by Ruppert (1995). We use a similar definition, presented by Amenta & Bern (1999), Amenta, Bern & Eppstein (1998), Amenta, Choi & Kolluri (2001), and Dey (2007).

We define the local feature size at a point  $\bar{\mathbf{x}} \in \mathbf{X}$ , denoted by  $\text{LFS}(\bar{\mathbf{x}})$ , as the Euclidean distance from  $\bar{\mathbf{x}}$  to the nearest point of the medial axis of  $\mathbf{X}$ .

The following definition of an  $\varepsilon$ -sample of the set  $\mathbf{X}$  (cf. Amenta, Choi & Kolluri (2001) and Dey (2007)) will be useful to describe a criterion for the sample density of points in  $\mathbf{X}$ , depending on the local behavior of the embedding  $\mathbf{x}(u, v)$ . Let  $\mathbf{P}_{\mathbf{x}} = \{\mathbf{x}_1, \mathbf{x}_2, \dots\}$  be a subset of  $\mathbf{X}$ . We call  $\mathbf{P}_{\mathbf{x}}$  an  $\varepsilon$ -sample of  $\mathbf{X}$  if, for each point  $\mathbf{p} \in \mathbf{X}$ , there exists a sample point  $\mathbf{x}_i \in \mathbf{P}_{\mathbf{x}}$ , such that  $\|\mathbf{p} - \mathbf{x}_i\| \leq \varepsilon \cdot \text{LFS}(\mathbf{p})$ .

### 3. The SEG metric framework

Let  $\mathbf{x} : \mathbb{R}^2 \rightarrow \mathbb{R}^m$ , with  $\mathbf{x}(u, v) = (x_1(u, v), \dots, x_m(u, v))$ , be a continuous one-to-one embedding as above. In addition, let  $r \mapsto d(r)$  for  $r \geq 0$  be a scalar-valued function (the scaling function), which is assumed to have the following properties:

- $d(0) = 0$ ,
- $d(r) > 0$  for  $r > 0$ ,
- $d'(r) \geq 0$  for  $r \geq 0$ , and
- $d(r)/r$  is monotonically decreasing for  $r > 0$ .

We define the distance  $D$  between two points  $\mathbf{u}_1 = (u_1, v_1)$  and  $\mathbf{u}_2 = (u_2, v_2)$  in  $\mathbb{R}^2$  as

$$D(\mathbf{u}_1, \mathbf{u}_2) = d(\|\mathbf{x}(u_1, v_1) - \mathbf{x}(u_2, v_2)\|). \quad (3.1)$$

**THEOREM 1.** *The distance  $D$  given by (3.1) defines a metric on  $\mathbb{R}^2$ .*

*Proof.* For all  $\mathbf{u}_1, \mathbf{u}_2, \mathbf{u}_3 \in \mathbb{R}^2$ , the distance  $D$  has to satisfy the following conditions:

- (i)  $D(\mathbf{u}_1, \mathbf{u}_2) \geq 0$ ,
- (ii)  $D(\mathbf{u}_1, \mathbf{u}_2) = 0$  iff  $\mathbf{u}_1 = \mathbf{u}_2$ ,
- (iii)  $D(\mathbf{u}_1, \mathbf{u}_2) = D(\mathbf{u}_2, \mathbf{u}_1)$ , and
- (iv)  $D(\mathbf{u}_1, \mathbf{u}_3) \leq D(\mathbf{u}_1, \mathbf{u}_2) + D(\mathbf{u}_2, \mathbf{u}_3)$ .

Conditions (i) and (iii) are trivially fulfilled. To show condition (ii), we have to use the fact that the embedding  $\mathbf{x}(u, v)$  has no self-intersection, since the map  $\mathbf{x} : \mathbb{R}^2 \rightarrow \mathbb{R}^m$  is one-to-one. The triangle inequality (iv) remains to be shown. For the sake of brevity we denote the Euclidean distance  $\|\mathbf{x}(\mathbf{u}_i) - \mathbf{x}(\mathbf{u}_j)\|$  by  $\ell_{i,j}$ . Since the Euclidean metric satisfies the triangle inequality, we obtain

$$\ell_{1,3} \leq \ell_{1,2} + \ell_{2,3}.$$

Now we distinguish two cases.

- Case 1:  $(\ell_{1,3} \leq \ell_{1,2})$  or  $(\ell_{1,3} \leq \ell_{2,3})$ .

Since  $d'(r) \geq 0$  for  $r \geq 0$  we have

$$d(\ell_{1,3}) \leq d(\ell_{1,2}) \text{ or } d(\ell_{1,3}) \leq d(\ell_{2,3}),$$

which implies

$$d(\ell_{1,3}) \leq d(\ell_{1,2}) + d(\ell_{2,3}).$$

This shows the triangle inequality (iv).

- Case 2:  $\ell_{1,3} > \ell_{1,2}$  and  $\ell_{1,3} > \ell_{2,3}$ .

Since  $\frac{d(r)}{r}$  is monotonically decreasing we know that

$$\frac{d(\ell_{1,3})}{\ell_{1,3}} \leq \frac{d(\ell_{1,2})}{\ell_{1,2}} \text{ and } \frac{d(\ell_{1,3})}{\ell_{1,3}} \leq \frac{d(\ell_{2,3})}{\ell_{2,3}}.$$

Now we have

$$\begin{aligned} d(\ell_{1,2}) + d(\ell_{2,3}) &= \ell_{1,2} \frac{d(\ell_{1,2})}{\ell_{1,2}} + \ell_{2,3} \frac{d(\ell_{2,3})}{\ell_{2,3}} \geq \\ &\geq \ell_{1,2} \frac{d(\ell_{1,3})}{\ell_{1,3}} + \ell_{2,3} \frac{d(\ell_{1,3})}{\ell_{1,3}} = (\ell_{1,2} + \ell_{2,3}) \frac{d(\ell_{1,3})}{\ell_{1,3}} \geq \\ &\geq \ell_{1,3} \frac{d(\ell_{1,3})}{\ell_{1,3}} = d(\ell_{1,3}) \end{aligned}$$

which proves the triangle inequality (iv).

□

For  $m = 2$  or  $m = 3$ , the embedding  $\mathbf{x}(u, v)$  is a parametric surface without self-intersections in  $\mathbb{R}^2$  and  $\mathbb{R}^3$ , respectively. Two examples of possible scaling functions are

$$d(r) = ar \quad \text{or} \quad d(r) = a \ln(br + 1) \quad (3.2)$$

for suitable real constants  $a, b > 0$ .

With the help of the metric  $D$  in (3.1), we can define a generalized disk  $\tilde{B}_r(\mathbf{c})$  and a generalized circle  $\tilde{C}_r(\mathbf{c})$  with radius  $r > 0$  and center  $\mathbf{c} \in \mathbb{R}^2$ , which are given by

$$\tilde{B}_r(\mathbf{c}) = \{\mathbf{p} \in \mathbb{R}^2 \mid D(\mathbf{p}, \mathbf{c}) \leq r\}$$

and

$$\tilde{C}_r(\mathbf{c}) = \{\mathbf{p} \in \mathbb{R}^2 \mid D(\mathbf{p}, \mathbf{c}) = r\},$$

respectively. That means we have  $\partial\tilde{B}_r(\mathbf{c}) = \tilde{C}_r(\mathbf{c})$ .

The following two propositions specify conditions for the cases  $m = 2$  and  $m = 3$ , which guarantee that generalized disks and circles behave ‘topologically well’ in the sense, that they are topological disks and a topological circles, respectively. Proposition 3 follows directly from earlier results of Amenta, Bern & Eppstein (1998) and Dey (2007).

**PROPOSITION 2.** *Let  $m = 2$ ,  $\mathbf{c} \in \mathbb{R}^2$ , and  $r > 0$ . Then a generalized disk  $\tilde{B}_r(\mathbf{c})$  and a generalized circle  $\tilde{C}_r(\mathbf{c})$  are a topological disk and a topological circle, respectively.*

*Proof.* Since  $\mathbf{x}(u, v)$  is a continuous one-to-one embedding in  $\mathbb{R}^2$ , the assertion is trivially true. □

**PROPOSITION 3.** *Let  $m = 3$ ,  $\mathbf{c} \in \mathbb{R}^2$ ,  $r > 0$  and  $\bar{r} = d^{-1}(r)$ . If  $\bar{r} < \text{LFS}(\mathbf{x}(\mathbf{c}))$ , then a generalized disk  $\tilde{B}_r(\mathbf{c})$  and a generalized circle  $\tilde{C}_r(\mathbf{c})$  is a topological disk and a topological circle, respectively.*

*Proof.* This will be shown by proving the following equivalent statement. If  $\bar{r} < \text{LFS}(\mathbf{x}(\mathbf{c}))$ , then the intersection of a ball

$$B_{\bar{r}}(\mathbf{x}(\mathbf{c})) = \{\mathbf{p} \in \mathbb{R}^3 \mid \|\mathbf{p} - \mathbf{x}(\mathbf{c})\| \leq \bar{r}\}$$

and of a sphere

$$C_{\bar{r}}(\mathbf{x}(\mathbf{c})) = \{\mathbf{p} \in \mathbb{R}^3 \mid \|\mathbf{p} - \mathbf{x}(\mathbf{c})\| = \bar{r}\}$$

with the set  $\mathbf{X} = \mathbf{x}(\mathbb{R}^2)$  is a topological disk and a topological circle, respectively.

The proof will be similar to the one of Corollary 3 of Amenta, Bern & Eppstein (1998). We will need later Lemma 1.1 of Dey (2007), which can be rephrased for our situation as follows.

*If a ball  $B_{\bar{r}}(\mathbf{q}) = \{\mathbf{p} \in \mathbb{R}^3 \mid \|\mathbf{p} - \mathbf{q}\| \leq \bar{r}\}$  with  $\mathbf{q} \in \mathbb{R}^3$  and  $\bar{r} > 0$  intersects the set  $\mathbf{X}$  at more than one point where either (i)  $B_{\bar{r}}(\mathbf{q}) \cap \mathbf{X}$  is not a topological disk or (ii)  $\partial(B_{\bar{r}}(\mathbf{q})) \cap \mathbf{X}$  is not a topological circle, then a medial axis point of  $\mathbf{X}$  is in  $B_{\bar{r}}(\mathbf{q})$ .*

We will now prove the proposition by contradiction. Let  $B_{\bar{r}}(\mathbf{x}(\mathbf{c}))$  be a ball which does not intersect the set  $\mathbf{X}$  in a topological disk. Because of Lemma 1.1 of Dey (2007), the ball  $B_{\bar{r}}(\mathbf{x}(\mathbf{c}))$  contains a point  $\mathbf{p}$  of the medial axis of  $\mathbf{X}$  with  $\|\mathbf{p} - \mathbf{x}(\mathbf{c})\| \geq \text{LFS}(\mathbf{x}(\mathbf{c}))$  and hence we get  $\bar{r} \geq \text{LFS}(\mathbf{x}(\mathbf{c}))$ , which is a contradiction. A similar approach can be used for the case of the sphere  $C_{\bar{r}}(\mathbf{x}(\mathbf{c}))$ . □

As an example, Figure 1 displays generalized circles for different SEG metrics induced by embeddings into  $\mathbb{R}^3$ .

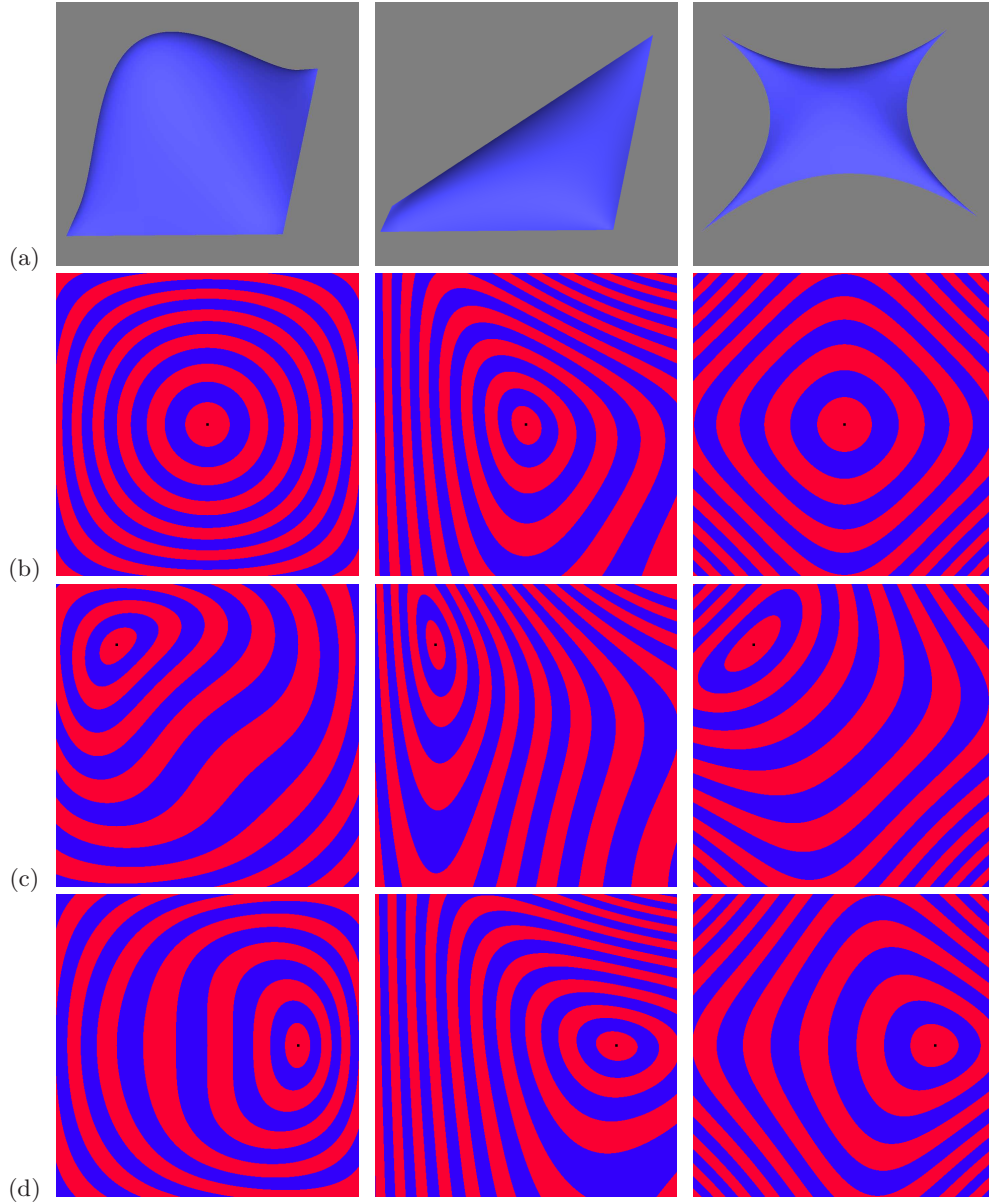


FIGURE 1. (a) Examples of embeddings into  $\mathbb{R}^3$  restricted to the parameter domain  $[0, 1]^2$ ; (b)-(d) Generalized circles for a uniform sequence of radii for different SEG metrics induced by the corresponding embeddings.

#### 4. Fitting SEG metrics to distance graphs

We now explain a method for computing suitable SEG metrics. The idea is to construct a spline embedding  $\mathbf{x}(u, v)$  which approximates a given distance graph best in the sense of least squares. The distance graph is used to specify a set of distances between points in the parameter domain.

We start with the definition of the distance graph. Then we explain the general framework of the fitting procedure, which is based on the Gauß-Newton algorithm. Finally we

modify this algorithm to ensure that the resulting embedding has no self-intersections, which is a necessary condition to induce a metric.

#### 4.1. Distance graph

Let  $\mathbf{I} = [0, 1]^2$  be the unit square, and let  $\mathbf{Q} = \{\mathbf{q}_1, \dots, \mathbf{q}_n\}$  be a set of points in  $\mathbf{I}$ . Further, let  $\mathbf{A}$  be a set of index pairs

$$\mathbf{A} = \{(\alpha, \beta)\} \subset \{1, \dots, n\}^2,$$

satisfying  $\alpha < \beta$  for all  $(\alpha, \beta) \in \mathbf{A}$ . Then a *distance graph*  $\mathcal{G}$  is given by the points of  $\mathbf{Q}$  and by the edges  $\mathbf{e}_{\alpha, \beta} = (\mathbf{q}_\alpha, \mathbf{q}_\beta)$ , for  $(\alpha, \beta) \in \mathbf{A}$ , with assigned edge lengths  $L_{\alpha, \beta}$ .

The lengths  $L_{\alpha, \beta}$  are not necessarily the Euclidean lengths of the corresponding edges  $\mathbf{e}_{\alpha, \beta}$ . Instead, we may consider generalized distances between the points  $\mathbf{q}_\alpha$  and  $\mathbf{q}_\beta$ .

A distance graph  $\mathcal{G}$  is said to be *valid* if the distances satisfy the generalized polygon inequality. That is, for each edge  $\mathbf{e}_{\alpha, \beta}$  the associated length  $L_{\alpha, \beta}$  is at most the length of any existing path from  $q_\alpha$  to  $q_\beta$  in the distance graph.

Though the generalized polygon inequality is no indispensable condition for the following surface fitting procedure to work, a significant deviation will cause inaccuracy of the approximation.

Several examples of valid distance graphs are shown in Figures 2, 4 and 5.

#### 4.2. Fitting procedure

The goal of this section is to construct an embedding which constitutes a least-squares approximation of a given distance graph. For simplicity, we choose the scaling function as  $d(r) = r$ . We are going to construct an embedding  $\mathbf{x}(u, v)$ , having a B-spline representation of degree  $(p_1, p_2)$ ,

$$\mathbf{x}(u, v) = \sum_{j=0}^{n_1} \sum_{k=0}^{n_2} \mathbf{c}_{j,k} M_j^{p_1}(u) N_k^{p_2}(v)$$

with control points  $\mathbf{c}_{j,k} \in \mathbb{R}^m$ . The respective basis functions  $(M_j^{p_1}(u))_{j=0, \dots, n_1}$  and  $(N_k^{p_2}(u))_{k=0, \dots, n_2}$  are B-splines of degree  $(p_1, p_2)$  with respect to the open knot sequences  $\mathcal{S} = (s_j)_{j=0, \dots, n_1+p_1+1}$  and  $\mathcal{T} = (t_k)_{k=0, \dots, n_2+p_2+1}$ , respectively.

Note that the embedding is only defined for the unit square  $[0, 1]^2$  which contains the given points. However, it could be extended to the entire plane  $\mathbb{R}^2$  with the help of suitable extrapolation techniques.

We compute the unknown coefficients  $\mathbf{c} = (\mathbf{c}_{0,0}, \dots, \mathbf{c}_{n_1,0}, \mathbf{c}_{1,0}, \dots, \mathbf{c}_{n_1,n_2})$  by solving the minimization problem

$$\mathbf{c} = \arg \min \sum_{(\alpha, \beta) \in \mathbf{A}} R_{\alpha, \beta}(\mathbf{c})^2, \quad (4.1)$$

where

$$R_{\alpha, \beta}(\mathbf{c}) = \|\mathbf{x}(\mathbf{q}_\alpha) - \mathbf{x}(\mathbf{q}_\beta)\|^2 - L_{\alpha, \beta}^2.$$

Since the optimization problem (4.1) is non-linear and the objective function is a sum of squares, we can use the Gauß-Newton algorithm to solve it. For each iteration step, we minimize the objective function

$$\left( \sum_{(\alpha, \beta) \in \mathbf{A}} (R_{\alpha, \beta}(\mathbf{c}^0) + \nabla R_{\alpha, \beta}(\mathbf{c}^0)(\Delta \mathbf{c} - \mathbf{c}^0))^2 \right) + \omega \|\Delta \mathbf{c} - \mathbf{c}^0\|^2, \quad (4.2)$$

which includes a Tikhonov regularization term, with respect to  $\Delta \mathbf{c}$ .

In the objective function (4.2), the vector  $\mathbf{c}^0$  denotes the solution from the last step,  $\Delta\mathbf{c}$  is the update, and  $\nabla R_{\alpha,\beta}$  is the row vector given by the partial derivatives of  $R_{\alpha,\beta}$  with respect to the control points  $\mathbf{c}_{j,k}$ . In addition,  $\omega > 0$  is the parameter for the Tikhonov regularization term.

For the first iteration step, we have to choose an initial solution for  $\mathbf{c}^0$ . This will be described in more detail in the next section.

Since the objective function (4.2) is quadratic in the update  $\Delta\mathbf{c}$ , we obtain a system of linear equations for  $\Delta\mathbf{c}$ . We repeat the minimization steps until  $\|\mathbf{c}^0 - \Delta\mathbf{c}\|$  is smaller than some chosen tolerance, or until we have exceeded a maximal (user-specified) number of iterations. In the latter case, we have still two possibilities to decrease the approximation error: We could increase the number of degrees of freedom of the B-spline representation by raising the number of control points or the degree of the B-splines, or we can increase the dimension of the embedding.

#### 4.3. Avoiding self-intersections

Since the construction from the previous section does not guarantee that the resulting embedding is free of self-intersections, we slightly modify the algorithm as follows.

The main idea is to construct an embedding  $\mathbf{x}(u, v) = (x_1(u, v), \dots, x_m(u, v))$  with  $m \geq 3$ , where the first two coordinate functions are simply linear functions with respect to  $u$  and  $v$ , respectively. That is, we put

$$x_1(u, v) = c^{(1)} u$$

and

$$x_2(u, v) = c^{(2)} v$$

with real coefficients  $c^{(1)}$  and  $c^{(2)}$ . The remaining coordinate functions  $x_i(u, v)$  for  $i \in \{3, \dots, m\}$  are spline functions of degree  $(p_1, p_2)$

$$x_i(u, v) = \sum_{j=0}^{n_1} \sum_{k=0}^{n_2} c_{j,k}^{(i)} M_j^{p_1}(u) N_k^{p_2}(v)$$

with  $c_{j,k}^{(i)} \in \mathbb{R}$ .

By solving the minimization problem (4.1) with the help of the Gauß-Newton algorithm as described in the previous section, we obtain an embedding  $\mathbf{x}(u, v)$  which has no self-intersections, as long as none of the coefficients  $c^{(1)}$  and  $c^{(2)}$  becomes zero in the optimization process. To avoid this case, we allow the user to specify the coefficients in our implementation. On the one hand the coefficients should not be chosen too large to make an approximation of the distance graph possible, on the other hand a choice of too small coefficients could lead in Section 5 to a SEG metric Voronoi diagram with a lot of orphans. Depending on the given distance graph we have tested different coefficients to find a satisfying choice. We have used this approach in all the presented examples below.

The use of these two linear functions can be seen as some kind of regularization. By using sufficiently small coefficients (combined with a sufficiently large dimension of the embedding), one can minimize the influence of this regularization while still avoiding self-intersections of the embedding.

The remaining coefficients  $c_{j,k}^{(i)}$  of the initial solutions were chosen randomly from the interval  $[-0.1, 0.1]$ . We always used several initial values. Note that different initial solutions give different results, and we picked the best one. In our experience, however, the obtained approximate solutions were different but they produced approximations of the given distance graph of similar quality, which was measured by the approximation error.

Our resulting but restricted embedding  $\mathbf{x}(u, v)$  induces a SEG metric on  $[0, 1]^2$ . By extending the restricted embedding to a continuous one-to-one embedding  $\mathbf{x} : \mathbb{R}^2 \rightarrow \mathbb{R}^m$ , we obtain a SEG metric on  $\mathbb{R}^2$ , which approximates the given distance graph.

We considered the scaling function  $d(r) = r$  for sake of simplicity. By choosing different scaling functions (for example as in (3.2)) it is possible to construct modified SEG metrics from the same distance graph. A similar optimization procedure could be applied to the parameters of the scaling functions  $d$ . However, this has not been implemented and tested.

In the following example we demonstrate the effect of our algorithm on the basis of the distance graph given in Figure 2. We approximated this discrete graph by a smooth spline embedding into  $\mathbb{R}^5$ . Examples of embeddings into  $\mathbb{R}^3$  resulting from other distance graphs are visualized in Figure 4.

We have summarized some details of the constructed spline embeddings, like the dimension  $m$ , the degree  $(p_1, p_2)$ , and the number of variable control points, for all our examples below (Examples 1 to 3) in Table 2. The numbers of executed iterations and the resulting relative errors are shown. The time for constructing all these spline embeddings is in the order of a few seconds, by using our non-optimized test software.

#### 4.4. Example 1

We consider the distance graph from Figure 2, which consists of 11 points  $\mathbf{q}_0, \dots, \mathbf{q}_{10} \in [0, 1]^2$  and of all possible edges  $(\mathbf{q}_\alpha, \mathbf{q}_\beta)$ . That is, the distance graph is the complete graph in this case. The assigned distances  $L_{\alpha, \beta}^{\text{real}}$  are given in the upper triangle of the distance matrix in Table 1. The overall sum of distances is 647.35.

We use our fitting algorithm from Section 4.3 to generate a cubic spline embedding into  $\mathbb{R}^5$ ; compare Table 2. As mentioned before, we have fixed both coefficients  $c^{(1)}$  and  $c^{(2)}$  as 1, and have chosen the remaining coefficients of the initial solution randomly. The projections of the resulting spline embedding into the 3-dimensional spaces  $x_1x_2x_3$ ,  $x_1x_2x_4$  and  $x_1x_2x_5$  are visualized in Figure 3. The lower triangle of the distance matrix in Table 1 shows the approximated distances  $L_{\alpha, \beta}^{\text{approx}}$  obtained from this embedding. The total error of the initial and approximated distances is

$$\sum_{(\alpha, \beta) \in \mathbf{A}} |L_{\alpha, \beta}^{\text{real}} - L_{\alpha, \beta}^{\text{approx}}| = 0.05.$$

This shows that the fitting algorithm for the approximation surface in  $\mathbb{R}^5$  led to a satisfactory result in this case.

## 5. SEG metric Voronoi diagrams

We will now use the metric  $D$  defined in (3.1) to construct a respective Voronoi diagram in  $\mathbb{R}^2$ , in a simple way.

Let  $\mathbf{P} = \{\mathbf{u}_1, \mathbf{u}_2, \dots\}$  be a set of sites in  $\mathbb{R}^2$ . The SEG metric Voronoi diagram  $V_D(\mathbf{P})$  for  $D$  can be generated in the following way. Given the sites  $\mathbf{u}_i \in \mathbb{R}^2$ , we first compute the corresponding points  $\mathbf{x}_i = \mathbf{x}(\mathbf{u}_i)$  on the embedding  $\mathbf{x}(u, v)$ , which has been used to define  $D$ . Then we compute, for the obtained set of points  $\mathbf{P}_\mathbf{x} = \{\mathbf{x}_1, \mathbf{x}_2, \dots\}$  in  $\mathbb{R}^m$ , their Euclidean Voronoi diagram  $V(\mathbf{P}_\mathbf{x})$ . By intersecting the resulting Voronoi cells with the embedding surface  $\mathbf{x}(u, v)$ , we obtain a Voronoi diagram on  $\mathbf{x}(u, v)$ , which defines for the corresponding parameter values  $(u, v) \in \mathbb{R}^2$  the desired SEG metric Voronoi diagram  $V_D(\mathbf{P})$  in  $\mathbb{R}^2$ .

This approach is similar to that in Boissonnat, Wormser & Yvinec (2008), who showed that the anisotropic Voronoi diagram of Labelle & Shewchuk (2003) can be obtained by intersecting a so-called power diagram in  $\mathbb{R}^5$  with a suitable surface. (Power diagrams

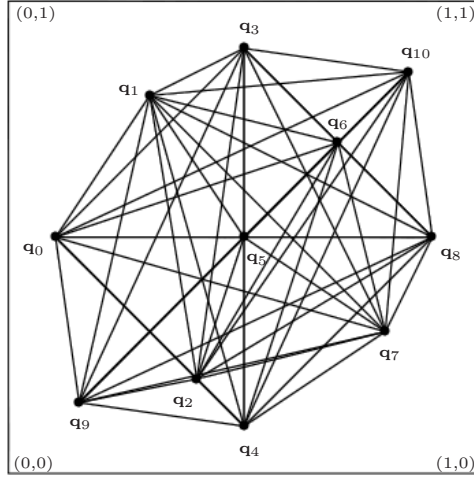


FIGURE 2. Complete distance graph on 11 points in  $[0, 1]^2$ . Distances are assigned as in Table 1.

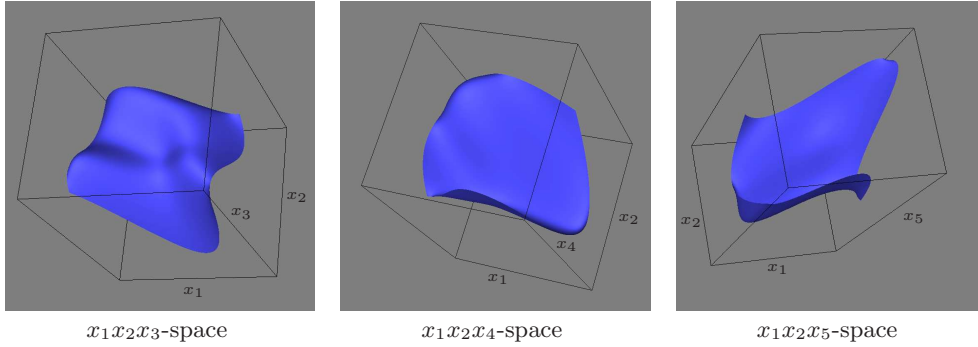


FIGURE 3. The resulting embedding projected to the 3-dimensional spaces  $x_1x_2x_3$ ,  $x_1x_2x_4$  and  $x_1x_2x_5$ . The  $x_1$ - and  $x_2$ -directions are scaled by a factor of 10 for better visibility.

are generalized Voronoi diagrams whose cells are still polyhedral; see e.g. Aurenhammer & Klein (2000).)

Before discussing several instances of SEG metric Voronoi diagrams constructed with our approach in detail, let us give some conditions under which the SEG metric Voronoi diagram is orphan-free. Recall that a Voronoi diagram is called orphan-free if each of its Voronoi cells is connected. Disconnectedness of a cell in the SEG metric Voronoi diagram means that the corresponding  $m$ -dimensional (polyhedral) cell in the Euclidean Voronoi diagram intersects the embedding surface more than once.

LEMMA 4. *For  $m = 2$ , the SEG metric Voronoi diagram is always orphan-free.*

*Proof.* Since  $\mathbf{x}(u, v)$  is a smooth one-to-one embedding into  $\mathbb{R}^2$ , and the Euclidean Voronoi diagram  $V(\mathbf{P}_{\mathbf{x}})$  in  $\mathbb{R}^2$  has convex (hence connected) cells, the resulting SEG metric Voronoi diagram  $V_D(\mathbf{P}_{\mathbf{x}})$  is orphan-free, too.  $\square$

LEMMA 5. *Let  $m = 3$ , and assume that  $\mathbf{x}(u, v)$  is  $C^2$ -smooth. If the set of sites  $\mathbf{P}_{\mathbf{x}} = \{\mathbf{x}(\mathbf{u}_1), \mathbf{x}(\mathbf{u}_2), \dots\}$  is a 0.18-sample of the surface  $\mathbf{X} = \mathbf{x}(\mathbb{R}^2)$ , then the resulting SEG metric Voronoi diagram  $V_D(\mathbf{P})$  is orphan-free.*

	$\mathbf{q}_0$	$\mathbf{q}_1$	$\mathbf{q}_2$	$\mathbf{q}_3$	$\mathbf{q}_4$	$\mathbf{q}_5$	$\mathbf{q}_6$	$\mathbf{q}_7$	$\mathbf{q}_8$	$\mathbf{q}_9$	$\mathbf{q}_{10}$
$\mathbf{q}_0$		8.31	<b>7.35</b>	12.41	10.95	10.30	15.52	15.83	19.05	5.74	21.12
$\mathbf{q}_1$	8.31		12.69	4.58	9.85	<b>5.74</b>	10.10	16.31	17.03	12.17	15.13
$\mathbf{q}_2$	<b>7.34</b>	12.69		15.17	8.83	<b>10.95</b>	15.07	10.44	14.87	<b>5.00</b>	20.20
$\mathbf{q}_3$	12.41	4.58	15.17		10.10	5.10	6.71	15.78	15.00	15.26	11.05
$\mathbf{q}_4$	10.96	9.85	8.83	10.10		5.10	9.00	9.95	10.72	12.21	12.88
$\mathbf{q}_5$	10.30	<b>5.75</b>	<b>10.96</b>	5.10	5.10		<b>5.92</b>	11.70	11.70	12.37	10.95
$\mathbf{q}_6$	15.52	10.10	15.07	6.71	9.00	<b>5.91</b>		11.23	8.83	16.31	5.92
$\mathbf{q}_7$	15.83	16.31	10.44	15.78	9.95	11.70	11.23		5.66	13.04	14.59
$\mathbf{q}_8$	19.05	17.03	14.87	15.00	10.72	11.70	8.83	5.66		17.49	10.05
$\mathbf{q}_9$	5.74	12.17	<b>5.01</b>	15.26	12.21	12.37	16.31	13.04	17.49		22.02
$\mathbf{q}_{10}$	21.12	15.13	20.20	11.05	12.88	10.95	5.92	14.59	10.05	22.02	

TABLE 1. Upper triangle: The initially assigned distances  $L_{\alpha,\beta}^{\text{real}}$  for the edges  $(\mathbf{q}_\alpha, \mathbf{q}_\beta)$  of the distance graph in Figure 2. Lower triangle: The approximated distances  $L_{\alpha,\beta}^{\text{approx}}$  obtained from the resulting embedding, computed with our fitting algorithm. Bold lengths identify distances where  $L_{\alpha,\beta}^{\text{approx}}$  differs from  $L_{\alpha,\beta}^{\text{real}}$ .

*Proof.* It is sufficient to show that each Voronoi cell  $V^i(\mathbf{P}_\mathbf{x})$  of the Euclidean Voronoi diagram  $V(\mathbf{P}_\mathbf{x})$  in  $\mathbb{R}^3$  intersects the embedding  $\mathbf{x}(u, v)$  in a topological disk. Since  $\mathbf{x}(u, v)$  is a  $C^2$ -smooth embedding into  $\mathbb{R}^3$  and the set of sites  $\mathbf{P}_\mathbf{x}$  is a 0.18-sample of  $\mathbf{X}$  we can apply Lemma 3.10 of Dey (2007), which exactly states the desired fact.  $\square$

By choosing an appropriate spline function  $x_3$  in the graph fitting algorithm from Section 4.3, it is possible to construct a  $C^2$ -smooth embedding into  $\mathbb{R}^3$ , which satisfies the assumptions of Lemma 5.

Observe that the proofs of Lemmas 4 and 5 actually imply a stronger result. The regions in the SEG metric Voronoi diagram are not only connected but are simply connected, under the restrictions given there.

### 5.1. Example 2

We consider three different distance graphs as shown in Figure 4. For each graph we have constructed an embedding into  $\mathbb{R}^3$ , see (b) and Table 2, which induces an SEG metric, by approximating the corresponding graph. Based on these metrics, several examples of Voronoi diagrams for different sets of sites  $\mathbf{P}$  have been generated. We have used uniformly distributed sites in (c) and non-uniformly distributed sites in (d) and (e).

In the first example, the distance graph is given by a uniform quadrilateral mesh,

for which all edges have the same distance, except for one column where distances are longer. The resulting B-spline surface is elongated in this region and leads, in the case of uniformly distributed sites, to an SEG metric Voronoi diagram with ‘slimmer’ cells in the corresponding part of the domain.

The second distance graph is given by a uniform triangular mesh, where at two parts (bottom left and top right) the lengths of the edges are larger than those of the remaining edges. By using our fitting algorithm we get a B-spline surface with two ‘hills’ at these parts. For the case of uniformly distributed sites, we obtain an SEG metric Voronoi diagram with strongly curved Voronoi cells in the corresponding parts of the domain.

In the last example, the distance graph is a triangular mesh again. The length of every other of the edges connected with the center point is larger compared to the other distances. As a resulting embedding we obtain a B-spline surface with various ‘hills’. For uniformly distributed sites, the SEG metric Voronoi diagram contains many cells of disk-like shape.

Observe that in the case of uniformly distributed sites (c), for all examples the resulting SEG metric Voronoi diagrams are orphan-free, whereas for the non-uniformly distributed sites in (d) two examples contain orphans. By adding more sites to the diagrams in (d), we can obtain Voronoi diagrams which are orphan-free (e).

### 5.2. Example 3

We present further examples of SEG metric Voronoi diagrams, for the more involved distance graphs shown in Figure 5. To obtain SEG metrics with good approximations, we have generated spline embeddings into the higher-dimensional spaces  $\mathbb{R}^5$  and  $\mathbb{R}^7$ ; cf. Table 2. Resulting Voronoi diagrams are displayed for two different kinds of sets of sites, uniformly distributed in (b) and (c) and non-uniformly distributed in (d) and (e).

In the first example, the distance graph is given by a square with its two diagonals, with diagonal lengths set to only about one half of the Euclidean lengths. For uniformly distributed sites, Voronoi cells which are close to the corners of the square are elongated. In the last two examples we obtain SEG metric Voronoi diagrams containing various disk-like Voronoi cells again. For each such cell, the corresponding site is the closest one to a point of the distance graph.

In the cases of uniformly distributed sites (b) and (c) the Voronoi diagrams are orphan-free for all shown examples, whereas for the non-uniform distribution (d) one diagram has orphans. Again, we can obtain an orphan-free Voronoi diagram by adding further sites (e).

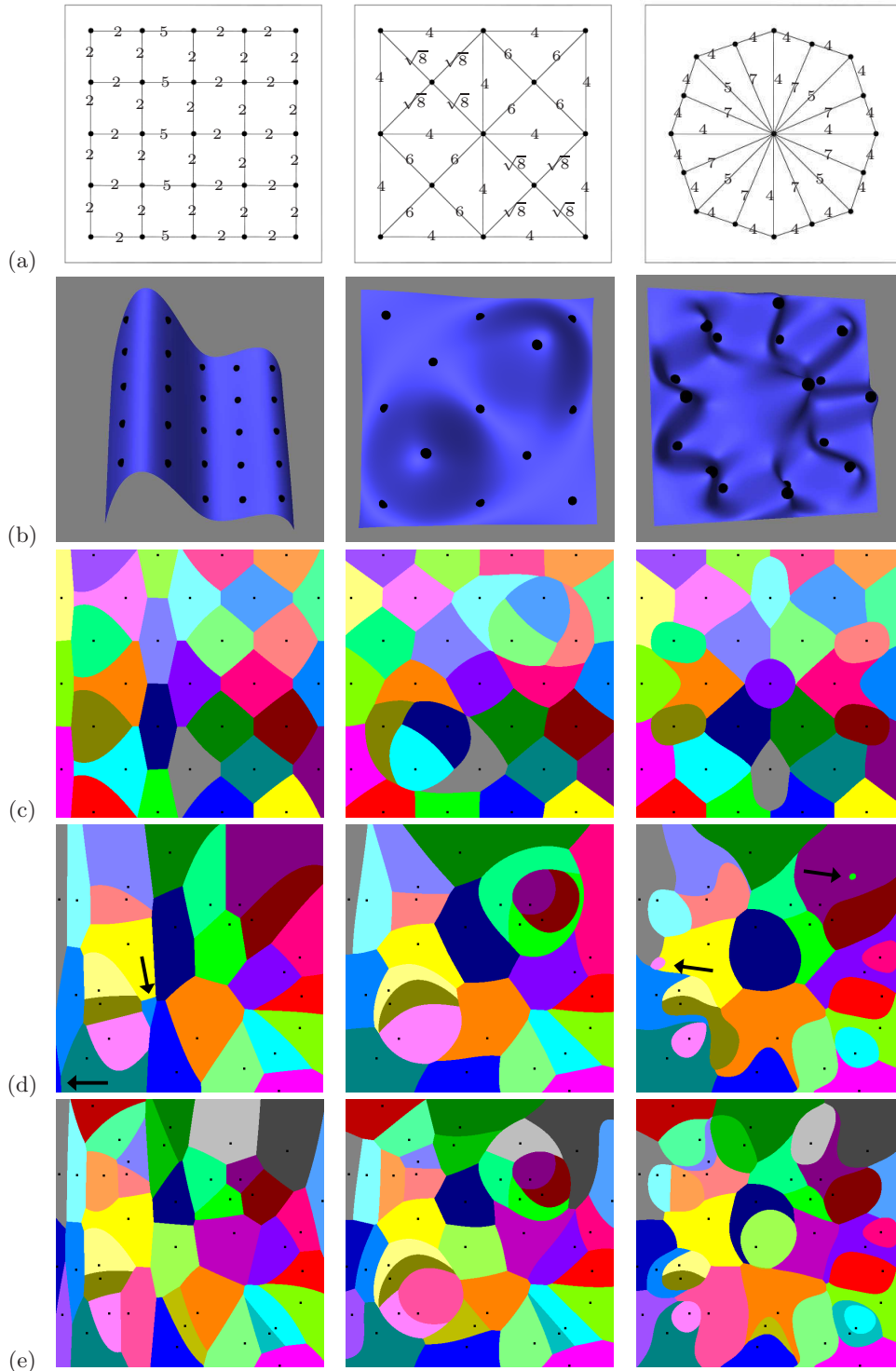


FIGURE 4. (a) Distance graphs; (b) Resulting embeddings into  $\mathbb{R}^3$ ; (c)-(e) Examples of SEG metric Voronoi diagrams for different sets  $\mathbf{P}$  of sites. Occuring orphans are indicated by arrows.



FIGURE 5. More distance graphs and their resulting SEG metric Voronoi diagrams for different sets of sites. Arrows indicate existing orphans. The metrics are induced by embeddings into  $\mathbb{R}^5$ ,  $\mathbb{R}^5$  and  $\mathbb{R}^7$ , respectively.

	Ex. 1	Ex. 2.1	Ex. 2.2	Ex. 2.3	Ex. 3.1	Ex. 3.2	Ex. 3.3
dimension $m$	5	3	3	3	5	5	7
degree $(p_1, p_2)$	(3, 3)	(3, 3)	(3, 3)	(3, 3)	(3, 3)	(3, 3)	(3, 3)
# contr. points	75	20	49	169	48	147	245
# iterations	15	40	40	18	12	26	32
relative error	$7.72 \cdot 10^{-5}$	$2.63 \cdot 10^{-3}$	$5.33 \cdot 10^{-4}$	$1.52 \cdot 10^{-2}$	$3.43 \cdot 10^{-8}$	$7.27 \cdot 10^{-8}$	$1.63 \cdot 10^{-7}$

TABLE 2. Some details of the constructed spline embeddings (Examples 1 to 3), the number of iterations, and the resulting relative errors  $(\sum_{(\alpha,\beta) \in \mathbf{A}} |L_{\alpha,\beta}^{\text{real}} - L_{\alpha,\beta}^{\text{approx}}|) / \sum_{(\alpha,\beta) \in \mathbf{A}} L_{\alpha,\beta}^{\text{real}}$ .

## 6. Concluding remarks

We have introduced the concept of scaled embedding-generated (SEG) metrics, and have studied some of their properties. SEG metrics are a versatile tool for reflecting the anisotropy specified by distance graphs in the plane. Also, they lead to a new type of generalized Voronoi diagram in  $\mathbb{R}^2$  in a canonical way.

Various questions remain open, for example, conditions under which Voronoi cells are connected (or simply connected), when the embedding is in dimensions higher than 3. In the non-orphan-free case, bounds on the number of connected Voronoi sub-cells are of interest.

Instead of the Voronoi diagram, also the generalized medial axis for shapes with respect to the disks defined by the new metric is worth studying.

## Acknowledgments

This work has been supported by the ESF EUROCORES Programme EuroGIGA - Voronoi, Austrian Science Foundation (FWF).

## REFERENCES

- AMENTA, N. & BERN, M. 1999 Surface reconstruction by Voronoi filtering. *Discrete & Computational Geometry* 22 (1999), 481–504.
- AMENTA, N., BERN, M. & EPPSTEIN, D. The crust and the beta-skeleton: Combinatorial curve reconstruction. *Graphical Models and Image Processing* 60 (1998), 125–135.
- AMENTA, N., CHOI, S. & KOLLURI, R.K. The power crust, unions of balls, and the medial axis transform. *Computational Geometry: Theory and Applications* 19 (2001), 127–153.
- AURENHAMMER, F. & EDELSBRUNNER, H. An optimal algorithm for constructing the weighted Voronoi diagram in the plane. *Pattern Recognition* 17 (1984), 251–257.
- AURENHAMMER, F. & KLEIN, R. Voronoi diagrams. In: J. Sack and G. Urrutia (eds.), *Handbook of Computational Geometry*, Elsevier, Amsterdam, 2000, 201–290.
- BOISSONNAT, J.-D., WORMSER, C. & YVINEC, M. Curved Voronoi diagrams. In: J.-D. Boissonnat and M. Teillaud (eds.), *Effective Computational Geometry for Curves and Surfaces*, Springer, Berlin, 2007, 67–116.
- BOISSONNAT, J.-D., WORMSER, C. & YVINEC, M. Anisotropic diagrams: Labelle Shewchuk approach revisited. *Theoretical Computer Science* 408 (2008), 163–173.
- CANAS, G.D. Practical conditions for well-behaved-ness of anisotropic Voronoi diagrams. *CoRR*, 2012.
- CANAS, G.D. & GORTLER, S.J. Duals of orphan-free anisotropic Voronoi diagrams are triangulations. *Proc. 28th Ann. ACM Symposium on Computational Geometry*, 2012, 219–228.
- CANAS, G.D. & GORTLER, S.J. Orphan-free anisotropic Voronoi diagrams. *Discrete & Computational Geometry* 46 (2011), 526–541.
- DEY, T.K. *Curve and Surface Reconstruction: Algorithms with Mathematical Analysis*. Cambridge Monographs on Applied and Computational Mathematics 23, Cambridge University Press, 2007.
- DU, Q. & WANG, D. Anisotropic centroidal Voronoi tessellations and their applications. *SIAM Journal on Scientific Computing* 26 (2005), 737–761.
- KUNZE, R., WOLTER, F.E. & RAUSCH, T. Geodesic Voronoi diagrams on parametric surfaces. *Proc. Conference on Computer Graphics International*, 1997, 230–237.
- LABELLE, F. & SHEWCHUK, J.R. Anisotropic Voronoi diagrams and guaranteed-quality anisotropic mesh generation. *Proc. 19th Ann. ACM Symposium on Computational Geometry*, 2003, 191–200.
- LETSCHER, D. Vector weighted anisotropic Voronoi diagrams and Delaunay triangulations. *Proc. 19th Ann. Canadian Conference on Computational Geometry*, 2007, 165–168.
- OKABE, A., BOOTS, B., SUGIHARA, K., CHIU, S.N. *Spatial Tessellations: Concepts and Applications of Voronoi Diagrams (2nd Edition)* John Wiley & Sons, Chichester, England, 2000.
- RUPPERT, J. A Delaunay refinement algorithm for quality 2-dimensional mesh generation. *Journal of Algorithms* 18 (1995), 548–585.